Pergamon

Computers Math. Applic. Vol. 32, No. 11, pp. 1–27, 1996

0898-1221/96 $15.00 + 0.00

PII: S0898-1221(96)00193-9

Signal Generation and Propagation in the Olfactory Bulb: Multicompartmental Modeling

I. ARADI
Department of Comparative Physiology, Eötvös University, Budapest
Múzeum krt. 4/A, H-1088 Budapest, Hungary
and
Department of Biophysics
KFKI Research Institute for Particle and Nuclear Physics of the Hungarian Academy of Sciences
P.O. Box 49, H-1525 Budapest, Hungary
aradi@sunserv.kfki.hu

P. ÉRDI
Department of Biophysics
KFKI Research Institute for Particle and Nuclear Physics of the Hungarian Academy of Sciences
P.O. Box 49, H-1525 Budapest, Hungary
erdi@rmki.kfki.hu

Abstract—The generation and propagation of action potentials in the two major cell types of the olfactory bulb, i.e., in the mitral and granule cells, are simulated by applying the multicompartmental modeling technique. The specific effects of the individual ionic currents, the propagation of the signals through the compartments, and several dynamic phenomena occurring in small networks (such as synchronized oscillation due to excitatory and inhibitory coupling) have been demonstrated.

Keywords—Single neuron dynamics, Neural simulation, Rhythmogenesis.

1. INTRODUCTION

The olfactory bulb is the first relay center of the olfactory system. Temporal, spatial, and spatiotemporal patterns formed by some self-organizing mechanisms are highly characteristic for the operation of the olfactory system [1]. Oscillatory and chaotic activities emerged in consequence of the interaction between mitral and granule cells. A detailed numerical bifurcation analysis of a network model of the olfactory bulb was given earlier [2,3]. The model network was built from relatively simple single cell elements.

Data of intracellular studies on the kinetics of voltage- and calcium-dependent ion channels have started to be available for different cells. Consequently, multicompartmental models supplemented with kinetic equations for the intrinsic membrane currents may be the building blocks of (moderately large) network models.

Simulation of detailed models of single mitral and granule cells (i.e., the main cell types of the olfactory bulb) have been done using morphological and electrophysiological data. Passive and active membrane data were either taken from Bhalla and Bower [4], who have already studied

We are grateful to P. Adorján for introducing us to use the NEURON software. The majority of the simulation has been done in K. Kaski's laboratory (Electronics, Tampere Univ. Technology) in the framework of the Hungarian-Finnish intergovernmental agreement (No. 7, National Committee for Technical Development). Support by the Hungarian Scientific Research Fund under Grant No. OTKA T 017784 is acknowledged.

many aspects of the dynamics of the mitral and granule cells, or were directly calculated from the original data found in the BABEL data base of the GENESIS user group [5]. In this work, we continue the analysis of these cells, and extend it to study also some dynamic phenomena produced in small networks of these connected cells.

Three types of problems have been studied:

(i) The effects of the individual currents and their role in the generation and suppression of action potentials, and in the control of firing frequencies.

(ii) Signal propagation through the compartments of both the mitral and granule cells have been simulated. The effects of both orthodromic and antidromic stimulation have been demonstrated.

(iii) The excitatory-inhibitory coupling between the mitral and granule cells through dendrodendritic synapses and the effects of the (partial) blockade of the GABAergic inhibition have been shown.

The elements of the multicompartmental modeling technique are briefly summarized in Section 2. Results of simulations of the mitral cells (Section 3) and of granule cells (Section 4) are presented. Elementary synaptic interactions and dynamic behaviour of small networks are analysed in Section 5. Some conclusions and future plans are mentioned in Section 6.

2. SOME ELEMENTS OF THE MULTICOMPARTMENTAL MODELING TECHNIQUE

The investigation of single neuron dynamics got a new impetus from at least two different directions. First, with the development of anatomical and electrophysiological methods both the axonal and dendritic branching patterns and the intrinsic physiological properties of different types of neurons became the subject of studies, and data to be incorporated into detailed models started to be available. Second, formal models have been used to demonstrate many phenomena interesting from the point of view of dynamical system theory, such as oscillation, multirhythmicity, burst, chaos, excitability, traveling waves, etc. The framework of single neuron dynamics is formulated by the Hodgkin-Huxley model [6], which describes the electrogenesis of the action potential, and more generally, the different spatiotemporal patterns. The spatiotemporal change of the membrane potential V is described by the extended cable equation

$$\tau \frac{\partial V}{\partial t} = \lambda^2 \frac{\partial^2 V}{\partial x^2} + R_m \left(I_l + \sum_{i=1}^{n} I_i + I_{\text{ext}} + I_{\text{syn}} \right), \tag{1}$$

where τ is the membrane time constant, λ is the cable length constant, R_m is the membrane resistance, I_l is the leakage current; $\sum_{i=1}^{n} I_i$ is the sum of the individual voltage-dependent ionic currents taken into account, I_{ext} is the input current, and I_{syn} is the synaptic current.

The general form for each type of ionic current is

$$I_i(t) = g_i^{\max} P_i(V(t)) \, (V(t) - E_i), \tag{2}$$

where $g_i^{\max}$ is the maximal conductance, $P_i(V(t))$ is the probability that the channel is open, and E_i is the equilibrium potential for the specific current. The leakage current can be written in the following form:

$$I_l = g_l \, (V(t) - E_l), \tag{3}$$

where g_l is the constant leakage conductance, and E_l is the leakage reversal potential.

Both single- and multicompartmental models exist. The crucial assumption behind a single-compartment model is that the whole cell can be characterized by a single membrane potential. The spatial distribution of channel densities and kinetics have been taken into account by using multicompartmental models. Techniques for simulating the behavior of branching neurons will be shown. All our simulations were performed on the NEURON simulator developed by Hines [7].

3. DYNAMICS OF THE MITRAL CELLS

3.1. Ionic Currents and Channel Kinetics

The mitral cell model has been assumed to contain six channel types, such as fast sodium (Na), fast delayed rectifier (K_f), slow delayed rectifier (K_s), transient outward potassium current (K_A), voltage- and calcium dependent potassium current (K_{Ca}), and L-type calcium current (L-Ca). The kinetics for each of the channel classes were obtained from the literature [4] and are not repeated here.

3.2. Intracompartmental Studies

In the following simulations, only one compartment with several segments has been taken into account. Within the whole compartment, the distribution of channel densities were uniform, but the potential values have been calculated in each segment. The approximately proper values of the maximal conductances were either taken from Bhalla and Bower [4], or were determined by some parameter estimation technique. The particular effect of the different ionic currents have been demonstrated by a series of simulations experiments.

In Figure 1 (see the Appendix for all figures), the meaning of the notion of 'neuron as a threshold unit,' is illustrated. As it can be seen, in Figure 1a, only subthreshold phenomenon appears, but in the case of Figure 1b, an action potential has been generated. In both cases, the external input was a short square-impulse function. The only source of the drastically different ("threshold") behavior is due to a small change in the value of the maximal conductance of the sodium current.

The role of the K_{Ca}-type channel and L-type calcium channel in the control of firing frequency can be seen in the Figures 2 and 3, respectively. The differences in the interspike intervals characterizing the firing rate of the cells is due to the differences in the maximal conductances. Increase of the maximal conductance tends to suppress of firing frequency. In these simulations, the external stimulus was taken as constant over time.

Mitral cells may exhibit bursting behaviour, if the calcium conductance is further increased and the parameters of the currents generating the fast spike are properly adjusted, as it is demonstrated in Figure 4. The number of peaks can be regulated even by adjusting g_{K_f}.

3.3. Signal Propagation through the Compartments

Detailed geometric data of the mitral cells were taken into account by adopting multicompartmental computer simulation techniques. Six compartments were considered, such as the soma, primary dendrite (or trunk), glomerular tuft, proximal secondary dendrite, distal secondary dendrite, and axon. Within each compartment uniform distribution of channel densities was assumed.

In Figures 5 and 6, the signal propagation through the compartments has been shown. In Figure 5, the current injection arrives to the soma, and it is constant over time. The strong size-sensitivity of the frequency of firing is demonstrated. Figure 6 shows the response of the cell for an antidromic stimulation arrived to the axon. As it can be seen, changes in the membrane potentials are different for each compartment due to the spatial ("compartmental") variations in channel densities. The larger frequency of the firing at the axon is due to its large sodium conductance, while the other compartments are entrained by the dynamics of the soma.

4. DYNAMICS OF THE GRANULE CELLS

4.1. Ionic Currents and Channel Kinetics

The granule cell model included five channel types: sodium (it is similar but different from the sodium current of the mitral cells), K_f, K_s, K_A, and noninactivating muscarinic potassium current (K_M). The channel kinetic data were taken from [4].

4.2. Intracompartmental Studies

The response of a granule cell both for short square impulse, and constant external stimulus were simulated (see Figures 7a and 7b, respectively). The underlying ionic currents were also visualized. The role of the only "new" type of ionic current, i.e., the muscarinic potassium current, has separately been studied, and demonstrated in Figures 8a,b. Slight increase in its maximal conductance leads to decrease of the firing frequency.

4.3. Signal Propagation through the Compartments

To take into consideration the geometry of the granule cell, four different regions with different channel densities, such as soma, trunk, peripheral dendrite, and deep dendrite, have been assumed. As usual, the channel densities were uniformly distributed within these compartments. Figures 9a–c show how the signal is propagated, and if the stimulus arrives to different parts of the cell, as the soma, peripheral dendrite, and deep dendrite, respectively.

5. ELEMENTARY SYNAPTIC INTERACTIONS AND SMALL NETWORKS

The dynamic behaviour of small networks built from these previously investigated cell types were studied by a series of simulations. The synaptic current is given as

$$I_{\mathrm{syn}}(t) = g_{\mathrm{syn}}(t)\,(V - E_{\mathrm{syn}})\,. \tag{4}$$

Here g_{syn} is the synaptic conductance, and E_{syn} is the synaptic reversal potential. The excitatory nature of the mitral-to-granule and the inhibitory character of the granule-to-mitral synaptic connections have been specified by the alpha function [8]:

$$g_{\mathrm{syn}}(t) = g_{\max}\left(\frac{t}{t_p}\right) e^{(1-(t/t_p))}. \tag{5}$$

Here the function g_{syn} increases to its maximum value of $g_{\max}$ at $t = t_p$. The values of the excitatory and inhibitory reversal potentials were set to 0 and $-95\,\mathrm{mV}$, respectively.

In Figure 10, the elementary dynamics of the excitatory-inhibitory loop, i.e., the effects of the synaptic connections between one mitral and one granule cell are investigated. The firing patterns of the disconnected cells are shown in Figure 10a. Mitral excitation implies the increase of the frequency of the granule cells (Figure 10b), while in Figures 10c,d, even the effects of the granular feedback are also included. Too large inhibition breaks down the rhythmic firing pattern, i.e., the blockage of inhibition implies the emergence of oscillation. These simulation results are in accordance with the physiological finding and suggestion, which states that the blockage of the GABA-ergic inhibition control the odour-induced activity [9,10].

The behaviour of a network of three mitral and three granule cells were simulated. In Figure 11a, isolated trains of spikes have been generated, while by increasing the excitatory effect the amplitude of the externally stimulated mitral cell exhibits a "waning-and-waxing" amplitude structure, which reminds of the spindle rhythms known in the thalamocortical system [11].

The self-excitation between mitral cells were also studied. GABA antagonists produce prolonged depolarization in the mitral cells [12,13], and the reentrant excitation in the mitral layer may be associated to a particular mode of bulbar rhythmogenesis. Figures 12 and 13 show the results of the behaviour of two mitral cells connected by mutual excitatory couplings. In the simulations shown in Figure 12, the stimulus was sustained, while in those shown in Figure 13, it was switched off in $t = 200\,\mathrm{ms}$. Figure 12a shows the firing patterns produced by the disconnected cells, and Figure 12b illustrates the appearance of a series of synchronized burst activity. Figure 13 displays that the increase of the strength of the excitatory coupling result in self-sustained activity.

Not only excitatory but also inhibitory coupling may lead to synchronized oscillation, as it happens, e.g., in the reticular nucleus of the thalamus [11].

Figure 14a shows the break down of the rhythmicity in the disconnected granule cells. A self-sustained synchronized oscillatory behaviour emerges, however, in case of mutual inhibitory coupling (Figure 14b) [14].

6. DISCUSSION

The results of the simulation experiments presented here show, in general, that the wealthy dynamic behaviour of single neurons should be understood based on detailed compartmental modeling studies using voltage- and calcium-dependent kinetic data. More specifically, hypotheses about the mechanism of the generation and propagation of many firing patterns of the mitral and granule cells have been tested, and approved or refined. Simulations of small networks suggest that not only the mitral-granule feedback loop, but the self-excitation in the mitral layer may be the anatomical substrate of bulbar rhythmogenesis. A whole-bulb model could and should be built based on detailed models of the single cells, and the simulation results on this model should compare with those obtained by our network model composed of "simple models" of the single cells [2,3].

REFERENCES

1. Ch. Skarda and W.J. Freeman, How brains make chaos in order to make sense of the world, *Behavioral and Brain Sciences* **10**, 161–195 (1987).
2. P. Érdi, T. Grőbler, G. Barna and K. Kaski, Dynamics of the olfactory bulb: Bifurcations, learning, and memory, *Biological Cybernetics* **69**, 57–66 (1993).
3. I. Aradi, G. Barna, P. Érdi and T. Grőbler, Chaos and learning in the olfactory bulb, *Int. J. Intelligent Systems* **10**, 89–117 (1995).
4. U.S. Bhalla and J.M. Bower, Exploring parameter space in detailed single neuron models: Simulations of the mitral and granule cells of the olfactory bulb, *J. Neurophysiology* **69**, 1948–1963 (1993).
5. J.M. Bower and D. Beeman, *The Book of GENESIS. TELOS, The Electronic Library of Science*, Springer-Verlag, (1995).
6. A. Hodgkin and A. Huxley, A quantitative description of membrane current and its application to conduction and excitation in nerve, *J. Physiology (London)* **117**, 500–544 (1952).
7. M. Hines, The NEURON simulation program, In *Neural Network Simulation Environments*, (Edited by Skrzypek), Kluwer Acad. Publ., Norwell, MA, (1993).
8. W. Rall, Distinguishing theoretical synaptic potentials computed for different soma-dendritic distribution of synaptic inputs, *J. Neurophysiology* **30**, 1138–1168 (1967).
9. P. Duchamp-Viret and A. Duchamp, GABAergic control of odour-induced activity in the frog olfactory bulb: Possible GABAergic modulation of granule cell inhibitory action, *Neuroscience* **56**, 905–914 (1993).
10. P. Duchamp-Viret, A. Duchamp and M. Chaput, GABAergic control of odor-induced activity in the frog olfactory bulb: Electrophysiological study with picrotoxin and bicuculline, *Neuroscience* **53**, 111–120 (1993).
11. M. Steriade, D.A. McCormick and T.J. Sejnowski, Thalamocortical oscillations in the sleeping and aroused brain, *Science* **262**, 679–685 (1993).
12. M.C. Nowycky, K. Mori and G.M. Shepherd, GABAergic mechanisms of Dendrodendritic synapses in isolated turtle olfactory bulb, *J. Neurophysiology* **46**, 639–648 (1981).
13. R. Nicoll and C.E. Jahr, Self-excitation of olfactory bulb neurones, *Nature* **296**, 441–444 (1982).
14. C. van Vreeswijk, L.F. Abbott and B. Ermentrout, When inhibition not excitation synchronizes neural firing, *J. Computational Neuroscience* **1**, 313–321 (1994).

APPENDIX

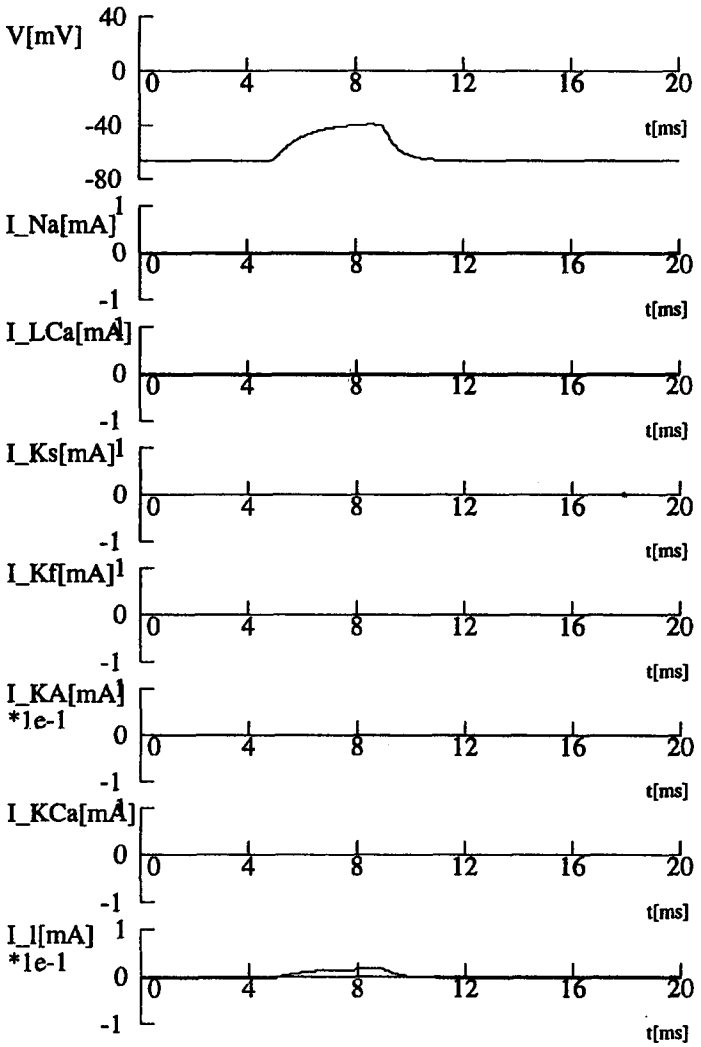

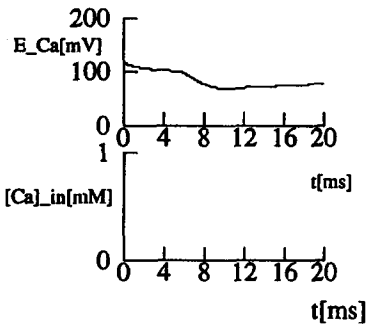

(a) $g_{\mathrm{Na}}^{\max} = 0.0312$ (S/cm^2).

Figure 1. Abrupt transition from subthreshold phenomenon (a) to action potential (b). Upper trace: the membrane potential. Lower traces: the underlying currents.

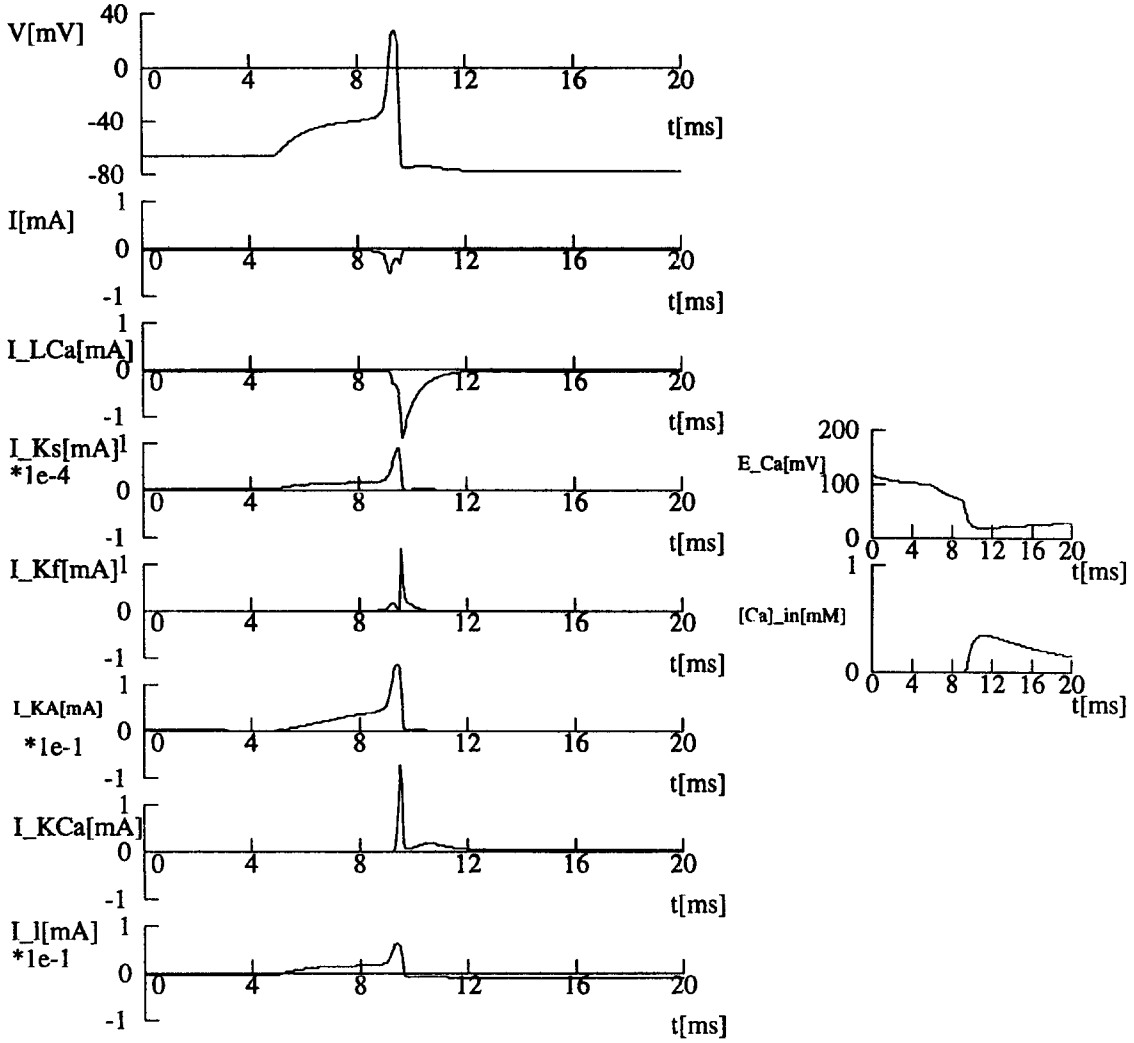

(b) $g_{\mathrm{Na}}^{\max} = 0.0313$ (S/cm^2).

Figure 1. (cont.)

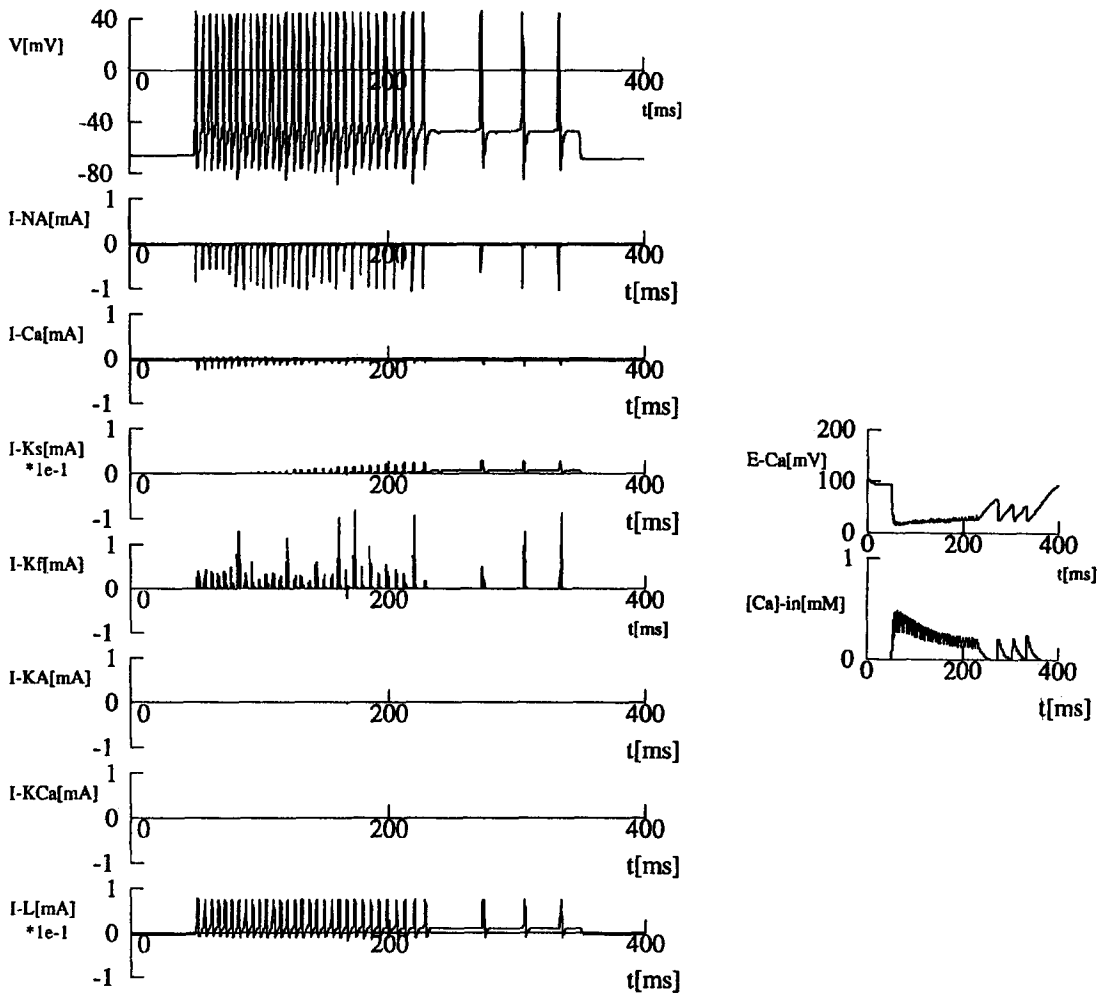

(a) 0 (S/cm^2).

Figure 2. Frequency control by changing $g_{\mathrm{K_{Ca}}}^{\max}$. Upper trace: the membrane potential. Lower traces: the underlying currents.

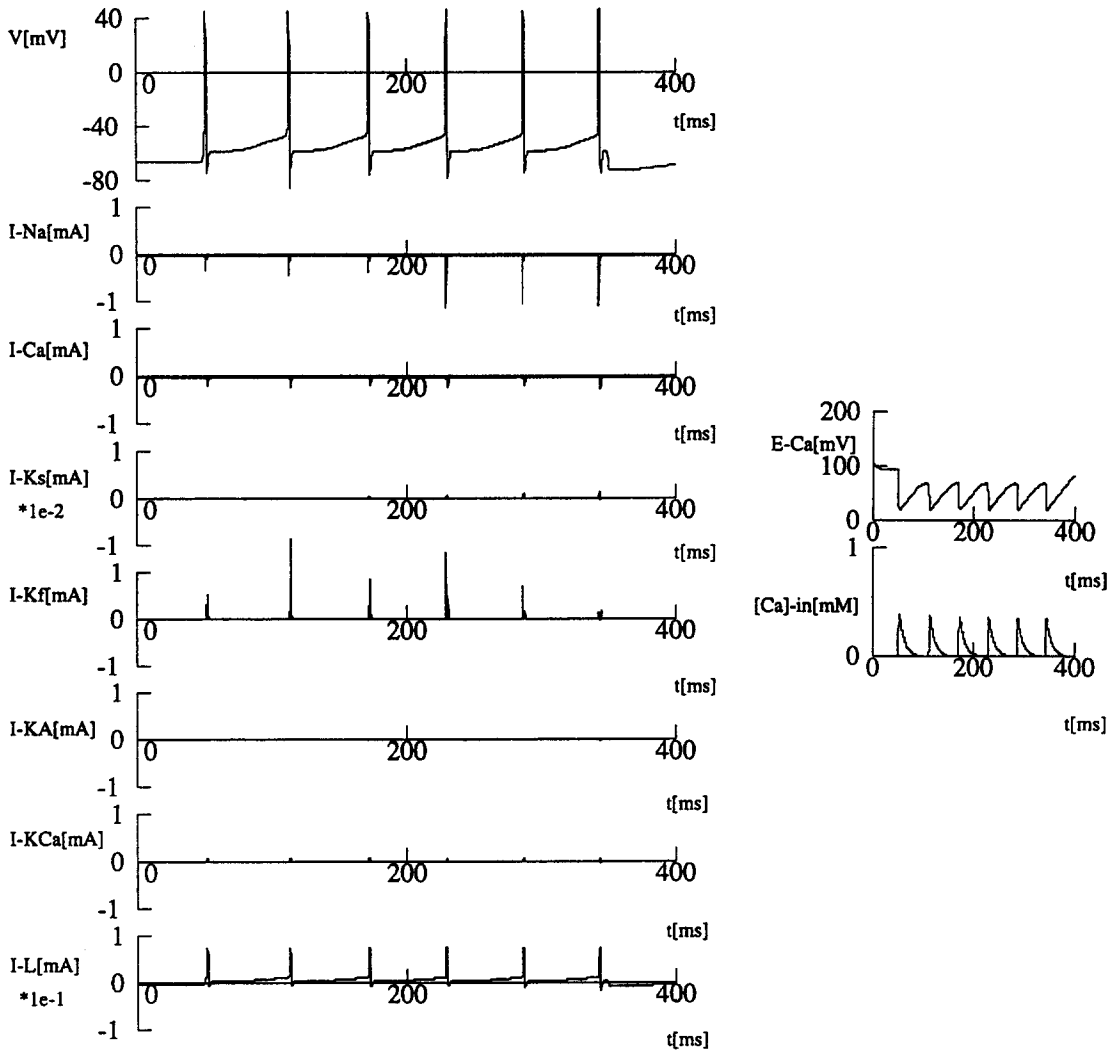

(b) 0.001 (S/cm^2).

Figure 2. (cont.)

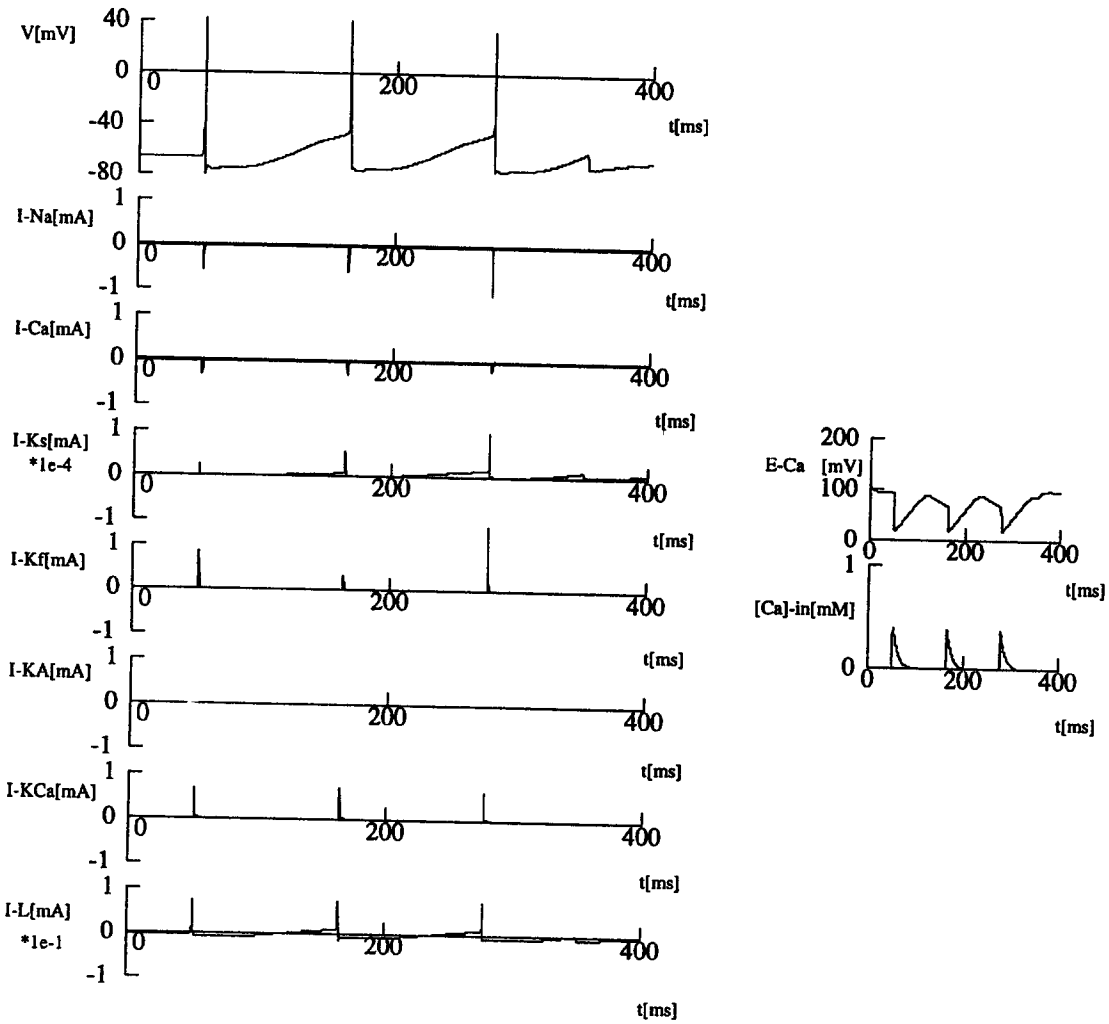

(c) 0.0142 (S/cm^2).

Figure 2. (cont.)

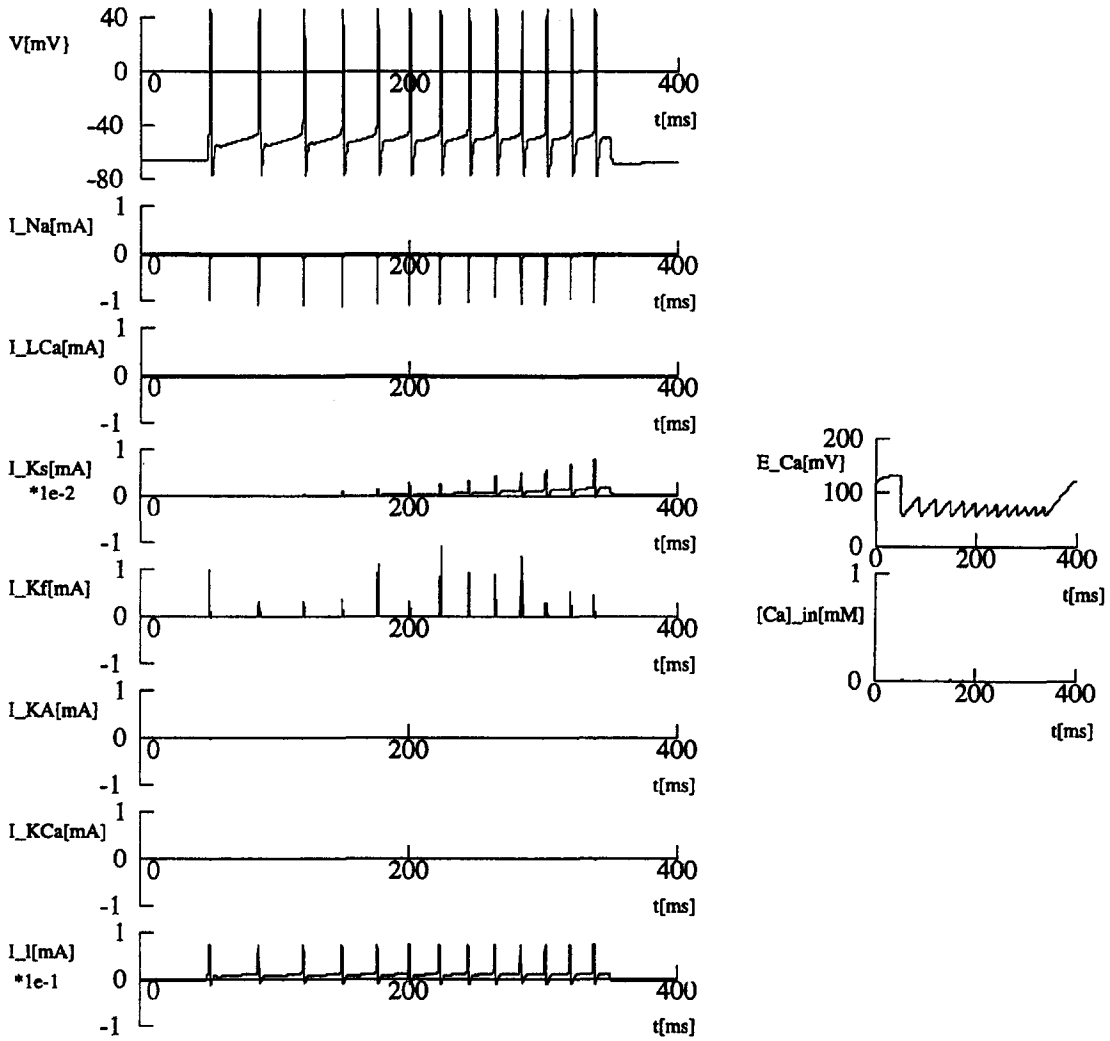

Figure 3. Frequency control by changing $g^{\max}_{\text{L-Ca}}$. The value of calcium conductance was set to 0.0001. See also Figure 2c, where $g^{\max}_{\text{L-Ca}} = 0.004$ (S/cm^2). Upper trace: the membrane potential. Lower traces: the underlying currents.

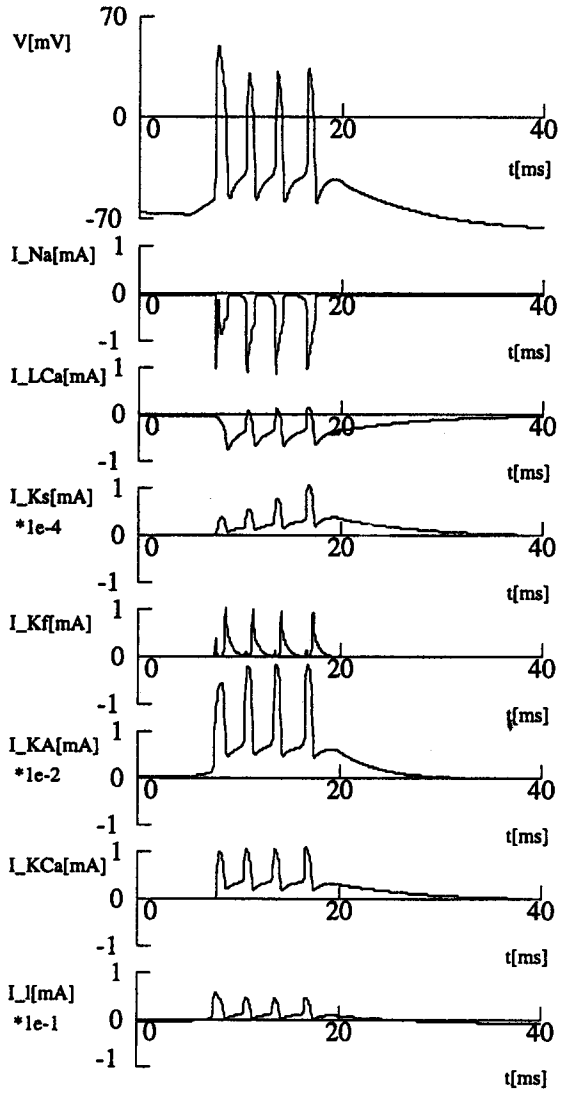

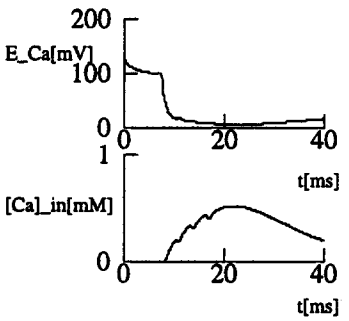

(a)

Figure 4. Intrinsic bursting behaviour of mitral cell can be obtained by increasing $g^{\max}_{\text{L-Ca}}$. The number of peaks is controlled by the $g^{\max}_{\text{K}_f}$. The values of the conductances of these channels were set to (a) $g^{\max}_{\text{L-Ca}} = 0.02$, $g^{\max}_{\text{K}_f} = 0.05$, and (b) $g^{\max}_{\text{L-Ca}} = 0.02$, $g^{\max}_{\text{K}_f} = 0.03$ (S/cm^2). The current injection lasted from the 5$^{\text{th}}$ to the 8$^{\text{th}}$ ms and its amplitude was 2 nA. Upper trace: the membrane potential. Lower traces: the underlying currents.

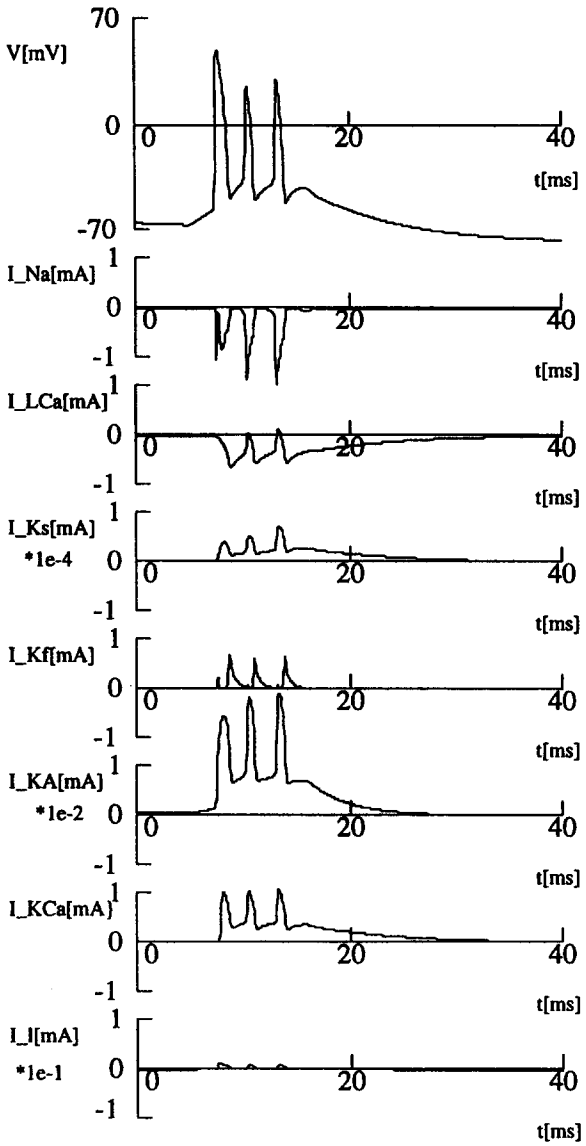

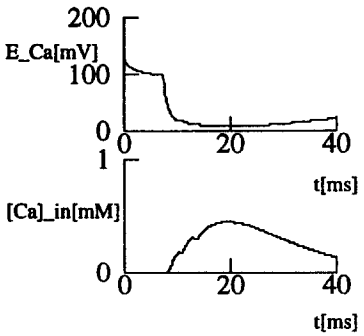

(b)

Figure 4. (cont.)

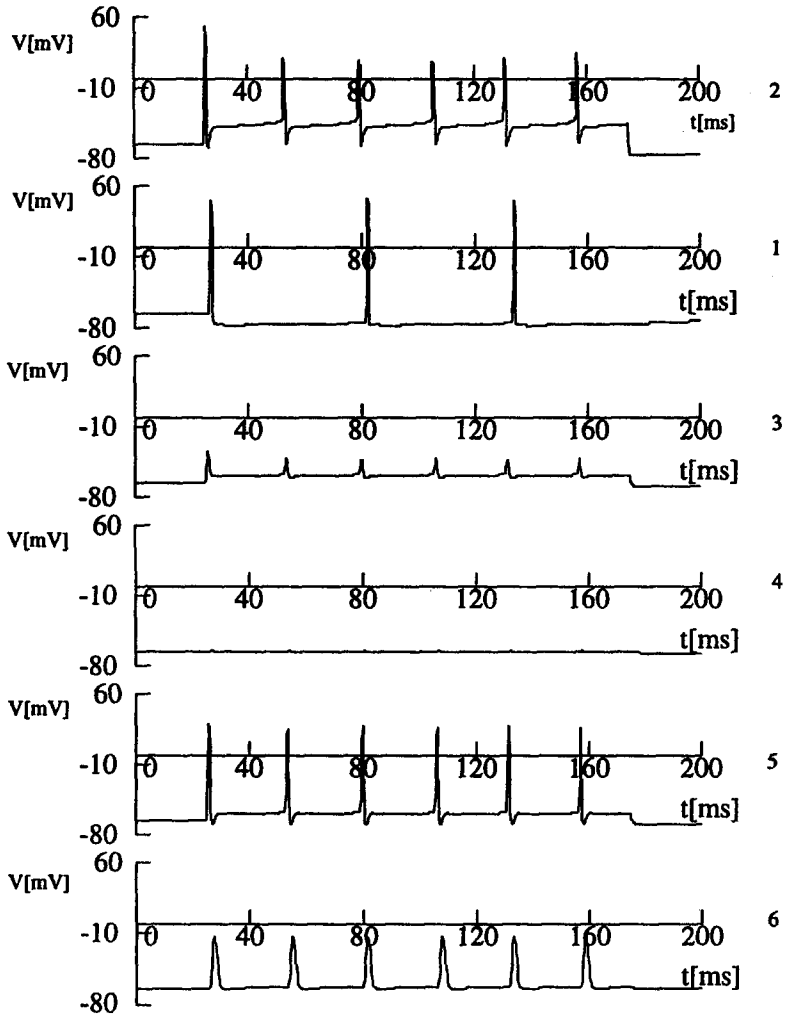

(a)

Figure 5. The demonstration of the sensitivity of the frequencies of the time patterns due to the lengths of the compartments. The values of the relative electrotonic lengths were set to (a) 2 (soma): 5; 1 (axon): 150; 3 (trunk): 30; 4 (peripheral dendrite): 30; 5 (proximal secondary dendrite): 30; 6 (distal secondary dendrite): 30. (b) 1. 300; 2. 300; 3. 100; 4. 100; 5. 100; 6. 100.

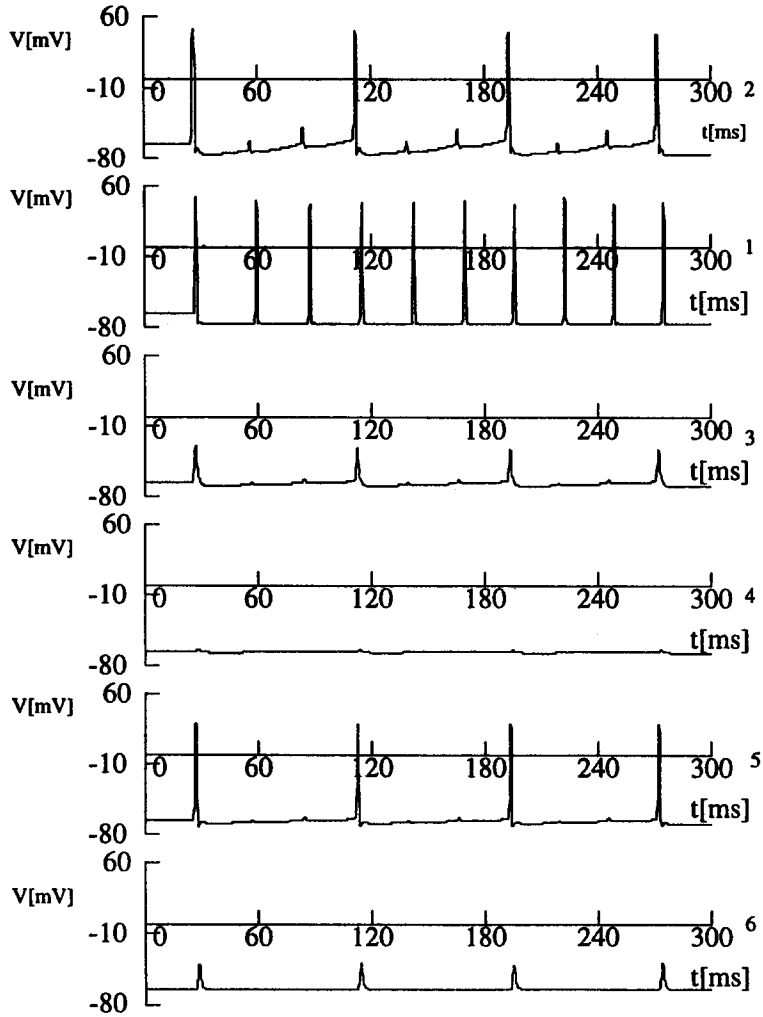

(b)

Figure 5. (cont.)

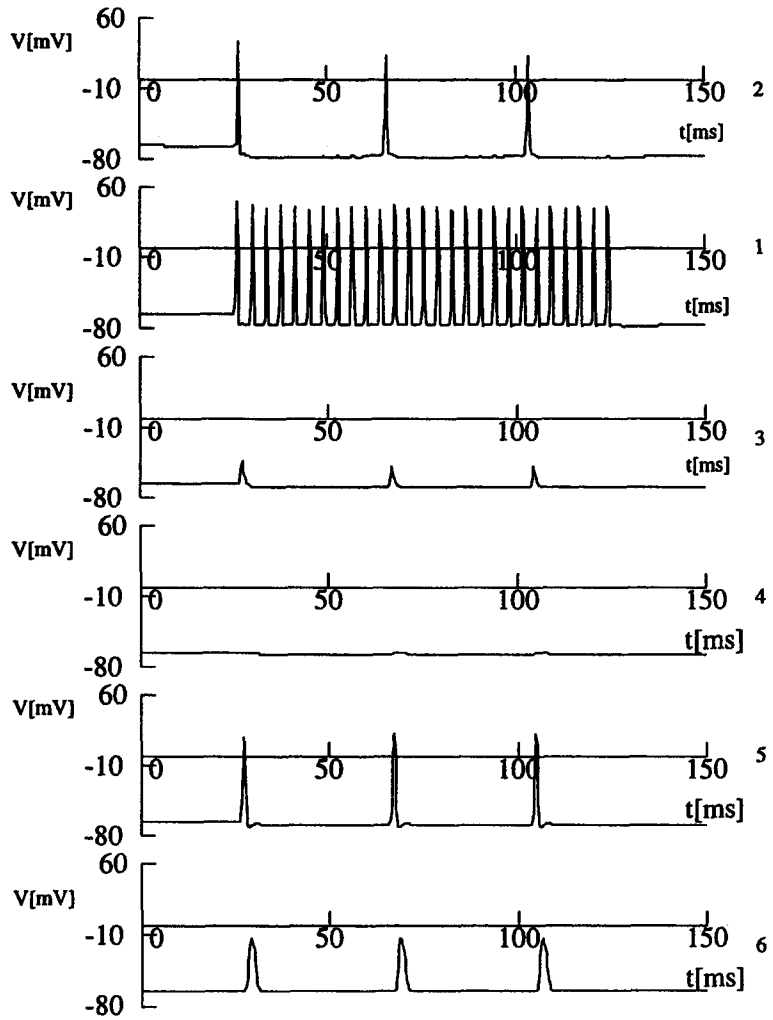

Figure 6. The response of the compartments for an axonic stimulation. The maximal values of the conductances were set to 2 (soma): $g_{\mathrm{Na}}^{\max} = 0.1532$, $g_{\mathrm{K}_f}^{\max} = 0.1956$, $g_{\mathrm{K}_s}^{\max} = 0.0028$, $g_{\mathrm{K}_A}^{\max} = 0.00587$, $g_{\mathrm{K_{Ca}}}^{\max} = 0.0142$; $g_{\mathrm{L\text{-}Ca}}^{\max} = 0.004$; 1 (axon): $g_{\mathrm{Na}}^{\max} = 0.4681$, $g_{\mathrm{K}_f}^{\max} = 0.1541$, $g_{\mathrm{K}_s}^{\max} = 0.00155$, $g_{\mathrm{K}_A}^{\max} = 0.00515$, $g_{\mathrm{K_{Ca}}}^{\max} = 0.00887$; $g_{\mathrm{L\text{-}Ca}}^{\max} = 0.002$; 3 (trunk): $g_{\mathrm{Na}}^{\max} = 0.00134$, $g_{\mathrm{K}_f}^{\max} = 0.00123$, $g_{\mathrm{K}_s}^{\max} = 0.00174$, $g_{\mathrm{L\text{-}Ca}}^{\max} = 0.0022$; 4 (primary dendrite): $g_{\mathrm{K}_s}^{\max} = 0.0028$, $g_{\mathrm{K}_A}^{\max} = 0.00587$, $g_{\mathrm{L\text{-}Ca}}^{\max} = 0.0095$; 5 (proximal secondary dendrite):$g_{\mathrm{Na}}^{\max} = 0.033$, $g_{\mathrm{K}_f}^{\max} = 0.0226$, $g_{\mathrm{K}_s}^{\max} = 0.00085$, $g_{\mathrm{L\text{-}Ca}}^{\max} = 0.0004$; 6 (distal secondary dendrite): $g_{\mathrm{Na}}^{\max} = 0.0122$, $g_{\mathrm{K}_f}^{\max} = 0.0128(\mathrm{S/cm^2})$.

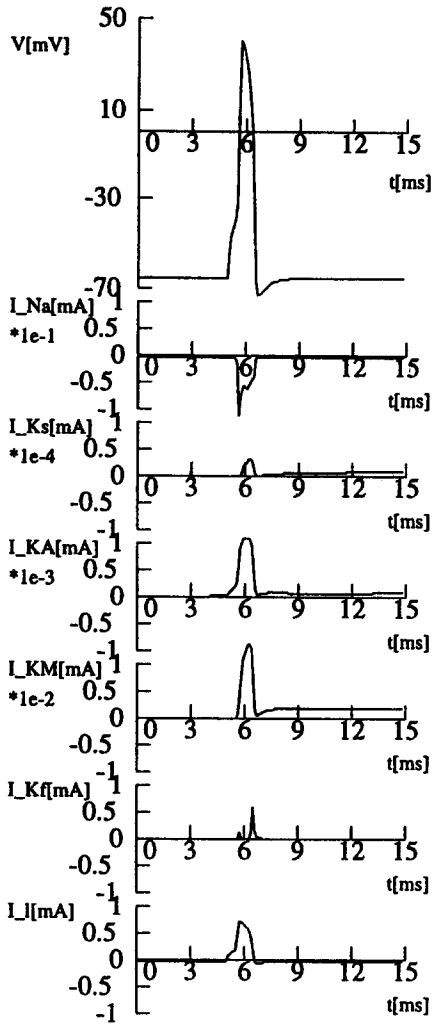

(a) Response for a small impulse stimulus by a single action potential.

Figure 7. Dynamics of the soma of the granule cell. Upper trace: the membrane potential. Lower traces: the underlying currents.

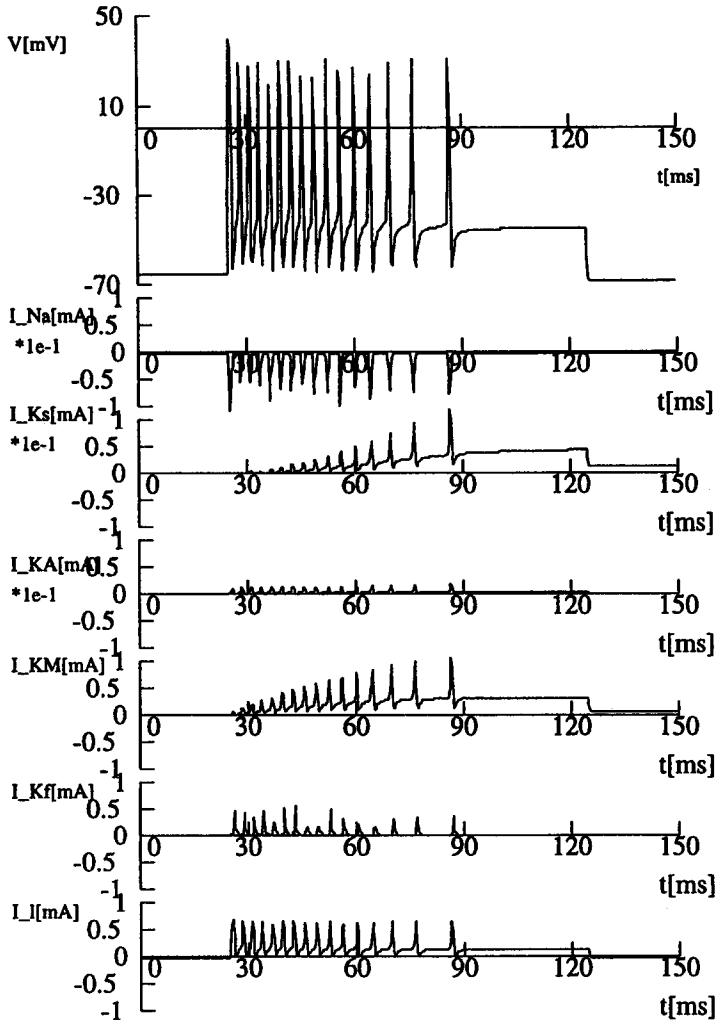

(b) Response for a constant stimulus by a spike-train.

Figure 7. (cont.)

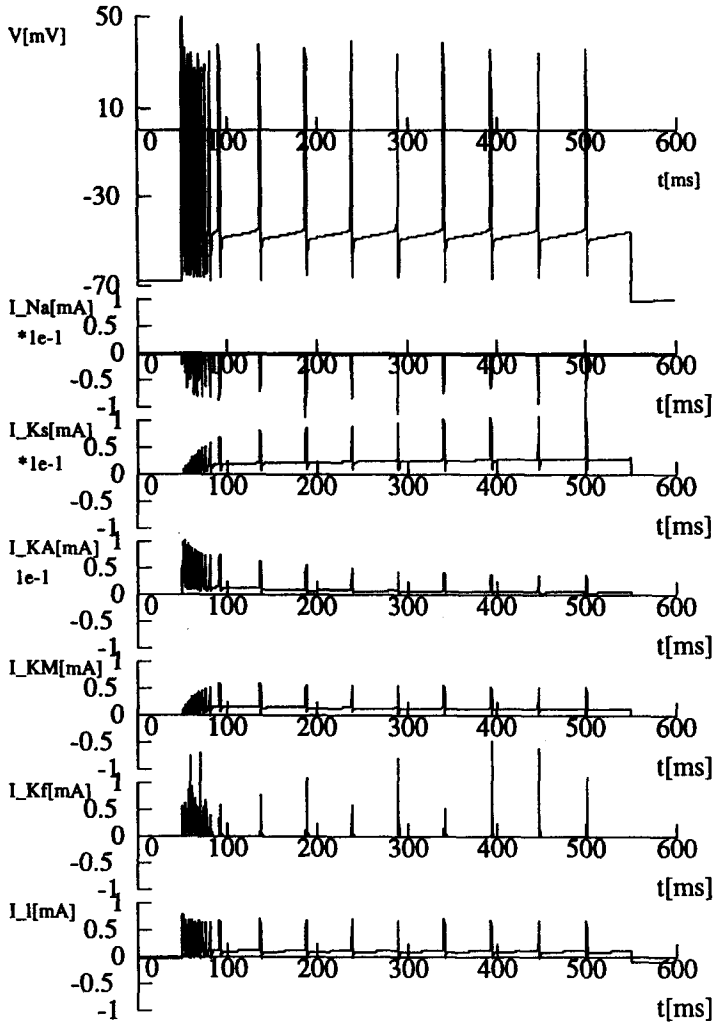

(a) $g_{K_M}^{max} = 0.03$ (S/cm^2).

Figure 8. The effect of the muscarinic type potassium conductance. Upper trace: the membrane potential. Lower traces: the underlying currents.

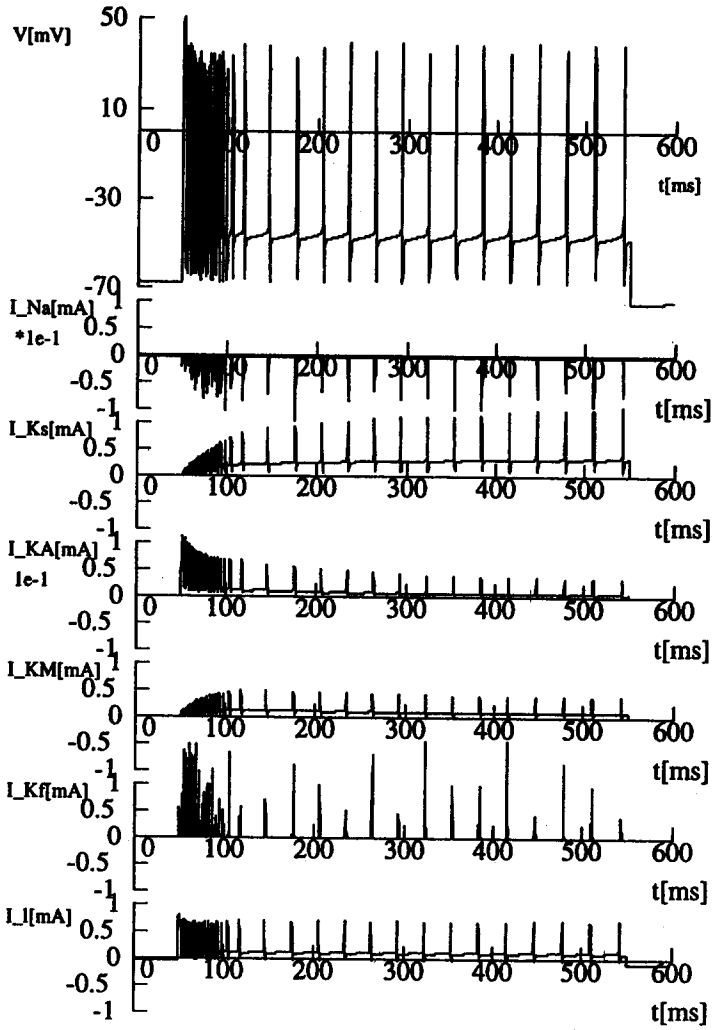

(b) $g_{K_M}^{max} = 0.035$ (S/cm^2).

Figure 8. (cont.)

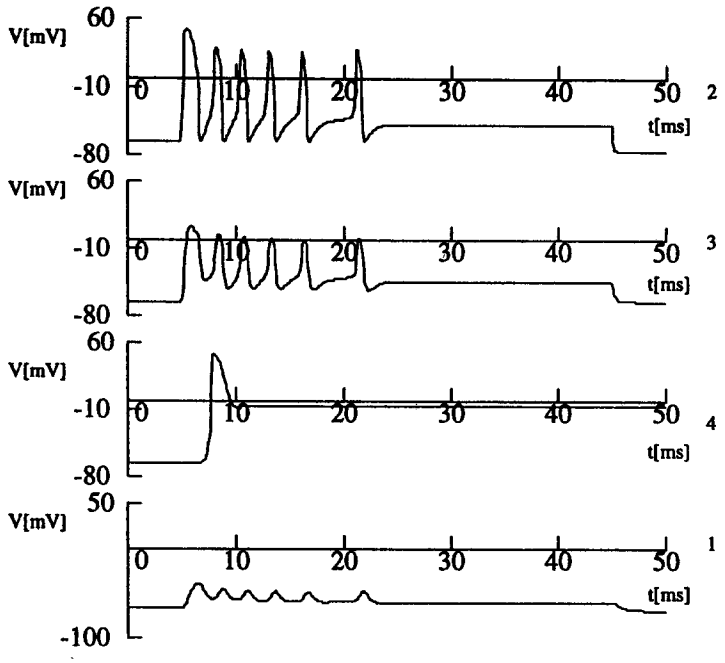

(a)

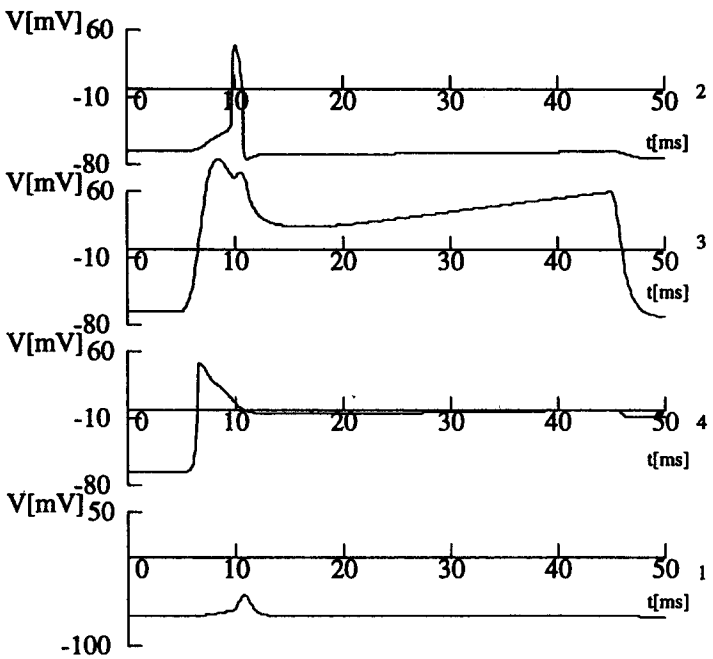

(b)

Figure 9. The spatial propagation of the stimulus arrived (a) for the soma, (b) for the peripherical dendrite, and (c) for the deep dendrite. According to the different channel densities, several activity patterns were generated in the different compartments. The maximal values of the conductances were set to 1 (soma): $g_{\mathrm{Na}}^{\max} = 0.1611$, $g_{\mathrm{K}_M}^{\max} = 0.1334$, $g_{\mathrm{K}_s}^{\max} = 0.1313$, $g_{\mathrm{K}_A}^{\max} = 0.0088$, $g_{\mathrm{K}_f}^{\max} = 0.05$; 2 (trunk): $g_{\mathrm{K}_s}^{\max} = 0.0071$; 3 (peripheral dendrite): $g_{\mathrm{Na}}^{\max} = 0.1355$, $g_{\mathrm{K}_s}^{\max} = 0.0243(\mathrm{S/cm^2})$; 4 (deep dendrite): considered as a passive cable.

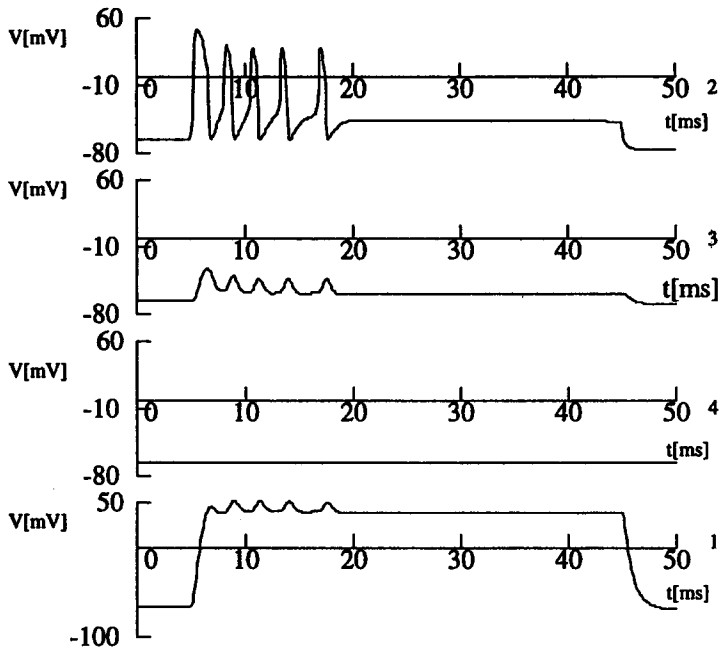

(c)

Figure 9. (cont.)

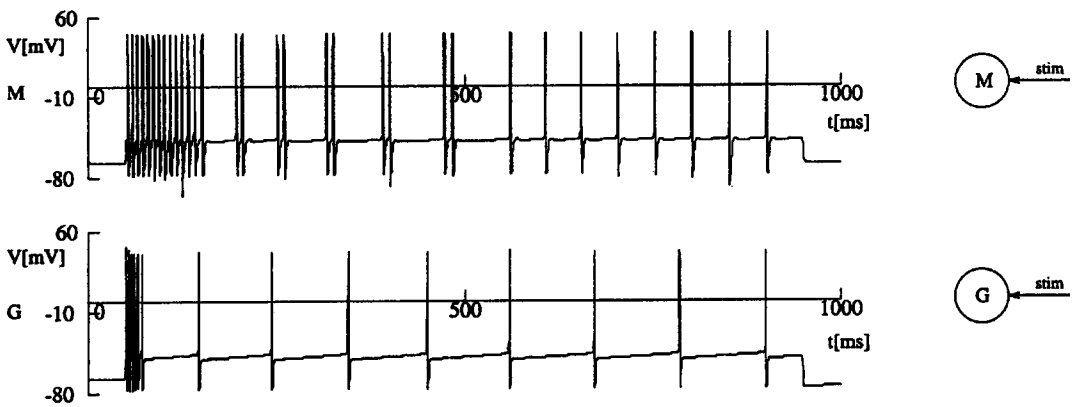

(a) Firing patterns of the disconnected cells.

Figure 10. Dynamics of the excitatory-inhibitory loop between a mitral and a granule cell.

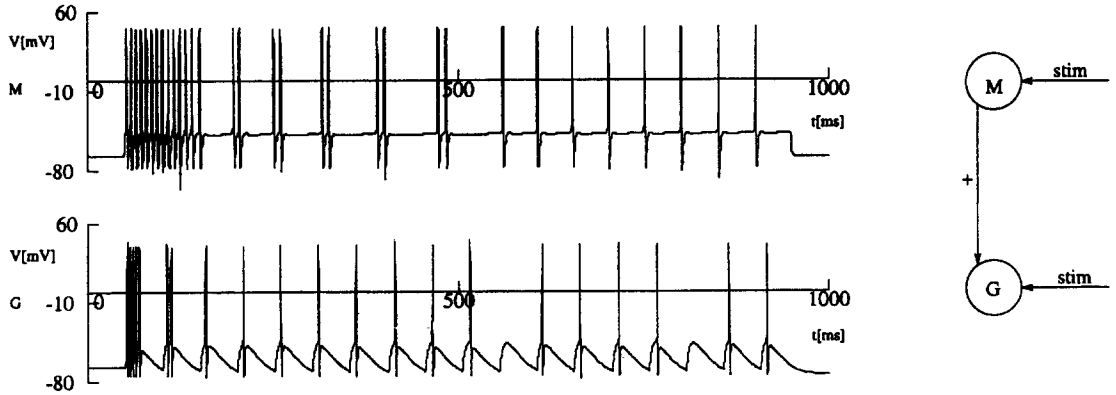

(b) Increase in frequency of the firing of the granule cells due to the excitation from the mitral cell $g_{\text{syn}} = 10$.

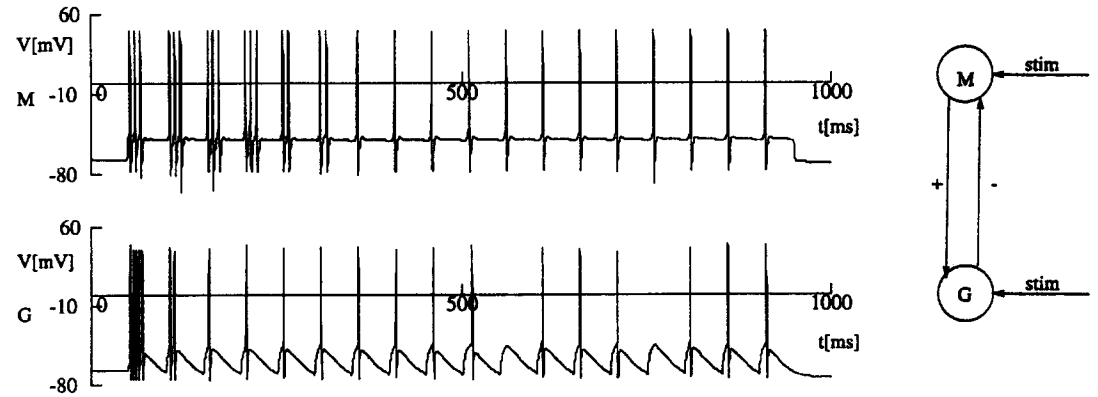

(c) The feedback effect of the granular inhibition to the mitral cell $g_{\text{syn}} = 50$.

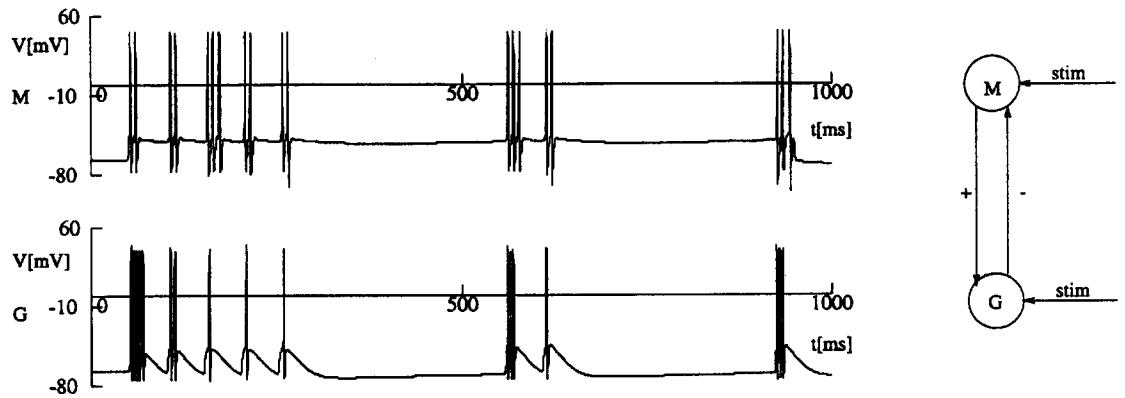

(d) Increased inhibition suppresses the rhythmic firing $g_{\text{syn}} = 85$ (pS).

Figure 10. (cont.)

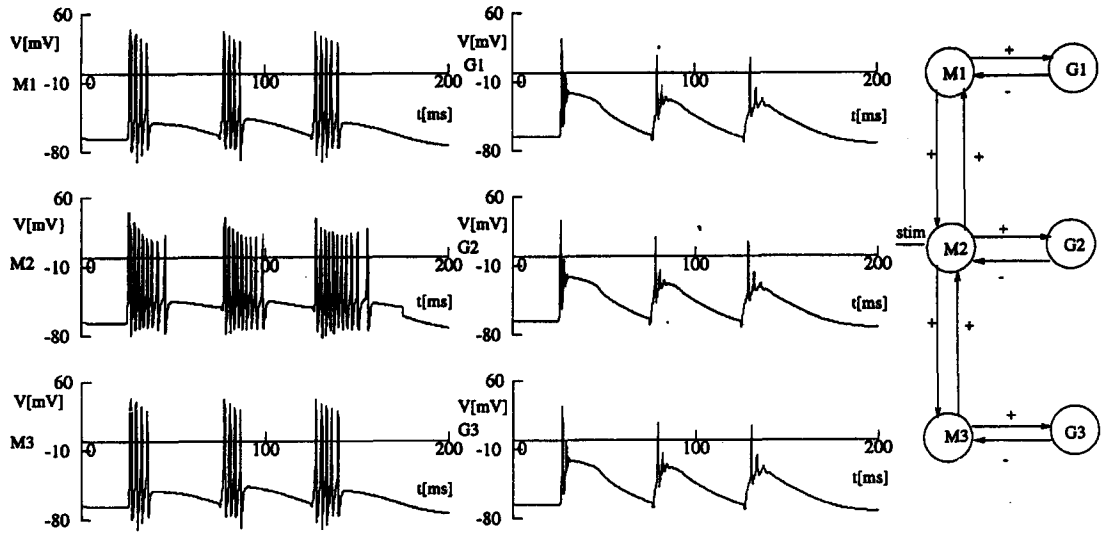

(a) "Small" excitation (the value of the synaptic conductance (g_{syn}) was set to 20 pS for m1-to-m2 and m3-to-m2 connections) implies the appearance of grouped trains of action potentials.

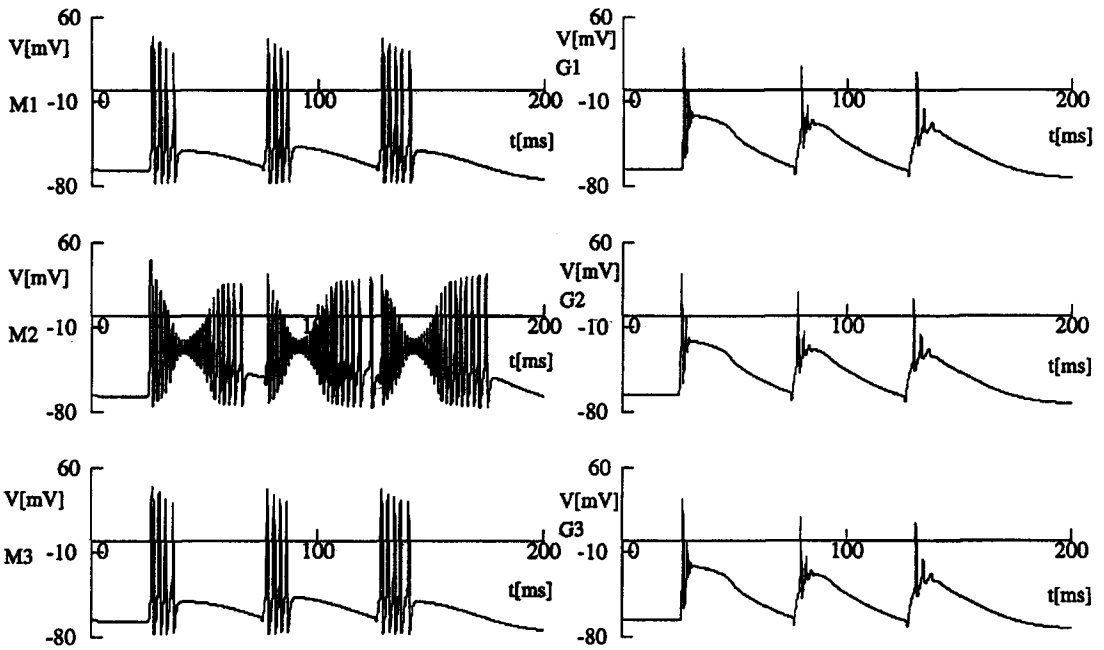

(b) "Increased" excitation ($g_{\mathrm{syn}} = 50$ pS) implies complex rhythmicity with "waning-and-waxing" amplitude pattern.

Figure 11. Dynamics of a small network built up from three mitral (m1, m2, m3) and three granule (g1, g2, g3) cells.

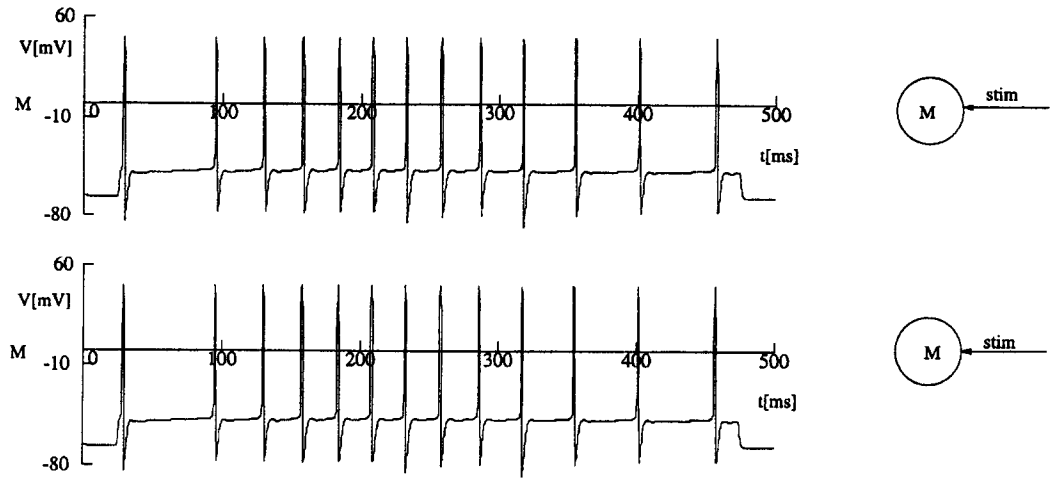

(a) Disconnected cells.

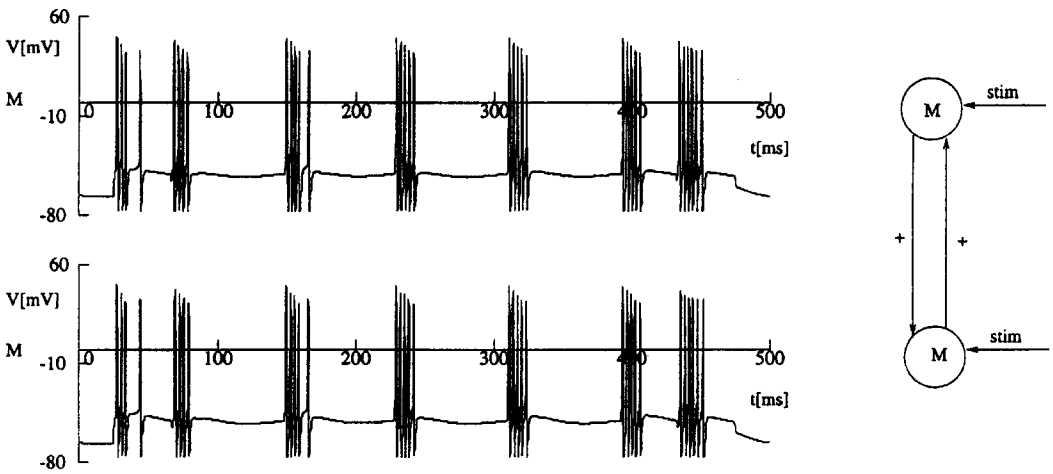

(b) The appearance of a series of synchronized bursting activity of two connected ($g_{\mathrm{syn}} = 5$ pS) cells.

Figure 12. Synchronized oscillation due to self-excitation as a response for a sustained stimulus.

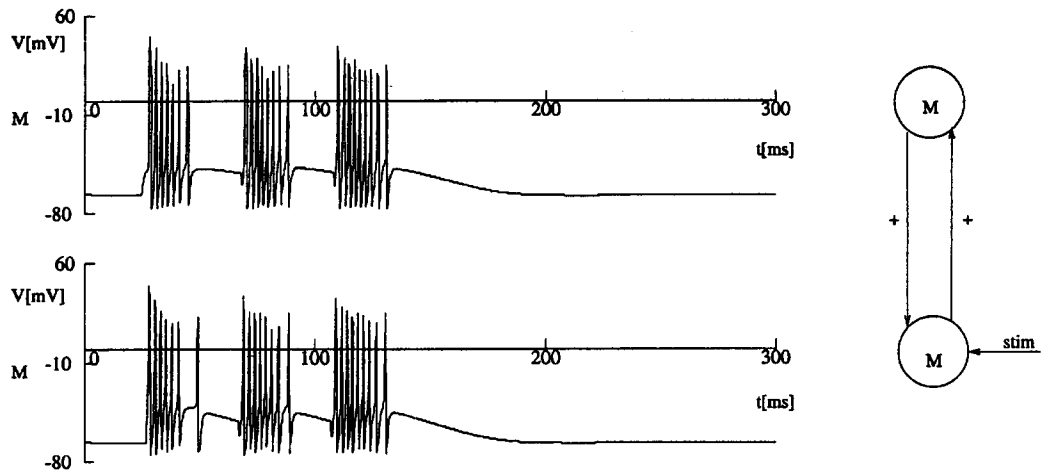

(a)

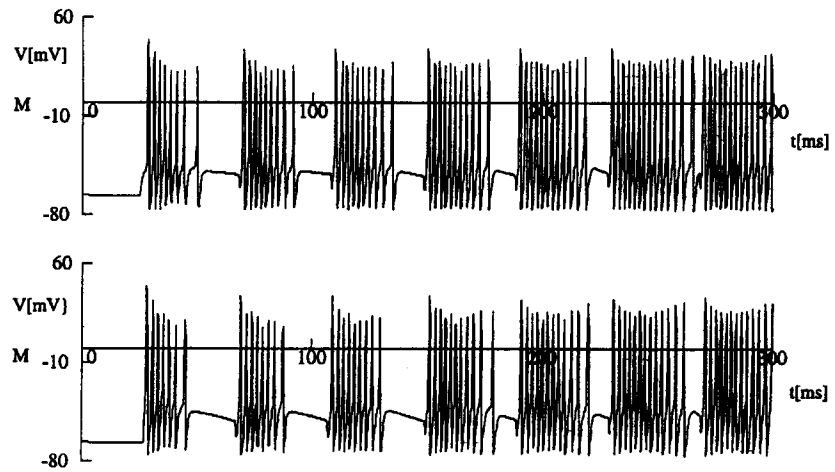

(b)

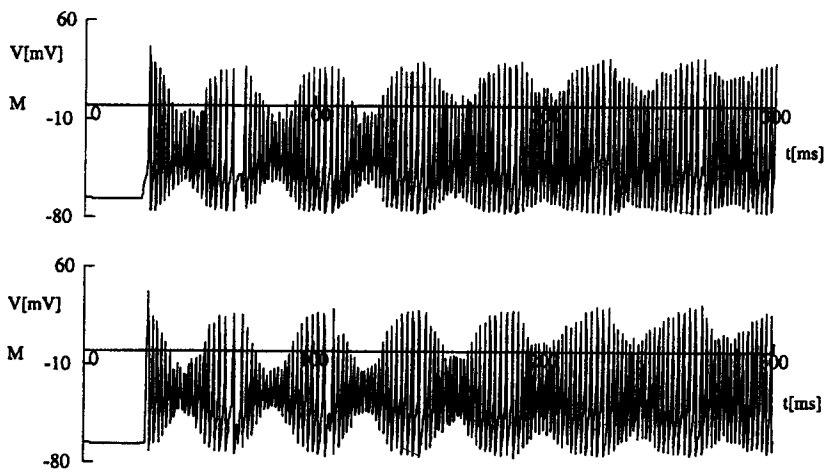

(c)

Figure 13. Synchronized oscillation due to self-excitation sustained after switching off the stimulus, if the synaptic coupling is larger than a threshold. The values of the mutual maximal synaptic conductances are (a) 30; (b) 40; (c) 100; and (d) 300 pS, respectively.

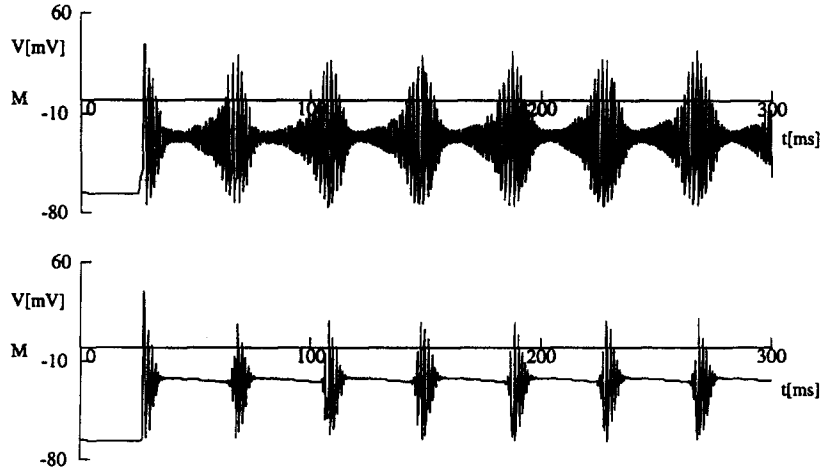

(d)

Figure 13. (cont.)

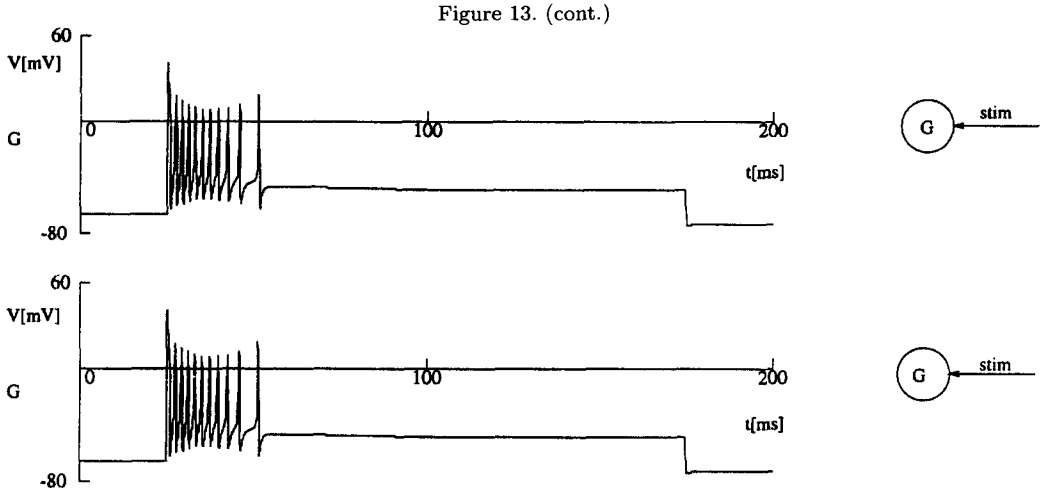

(a) The break down of rhythmicity in disconnected cells.

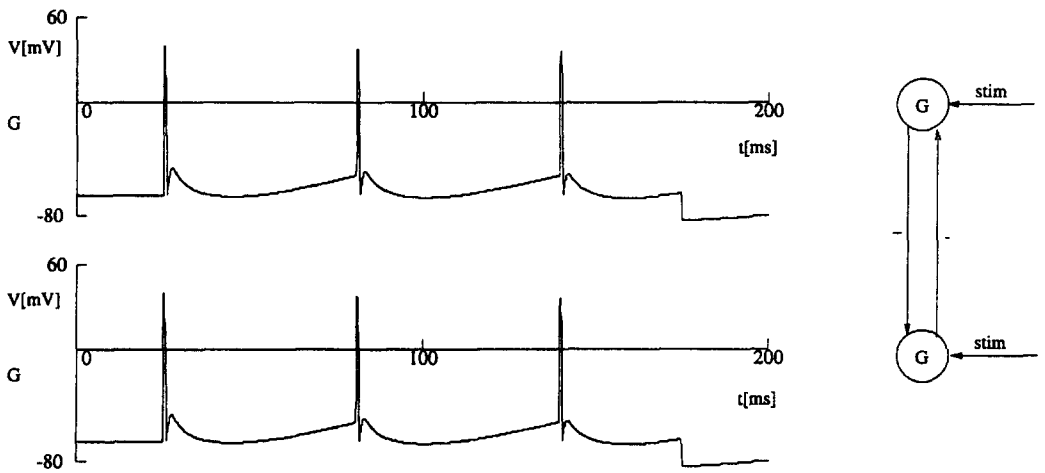

(b) Sustained synchronized activity of two coupled granule cells $g_{\mathrm{syn}} = 80$ pS.

Figure 14. Synchronized oscillation due to self-inhibition.